International Journal of Heat and Mass Transfer 52 (2009) 962–970

Contents lists available at ScienceDirect

International Journal of Heat and Mass Transfer

journal homepage: www.elsevier.com/locate/ijhmt

Turbulent flow and heat transfer in discrete double inclined ribs tube

Xiao-wei Li, Ji-an Meng *, Zeng-yuan Guo

School of Aerospace, Tsinghua University, Beijing 100084, PR China

ARTICLE INFO

Article history:
Received 11 July 2007
Received in revised form 24 March 2008
Available online 1 October 2008

Keywords:
Field synergy principle
Heat transfer enhancement
DDIR tube
Longitudinal vortex

ABSTRACT

The turbulent heat transfer and flow resistance in an enhanced heat transfer tube, the DDIR tube, were studied experimentally and numerically. Water was used as the working fluid with Reynolds numbers between 15,000 and 60,000. The numerical simulations solved the three dimensional Reynolds-averaged Navier–Stokes equations with the standard k-ε model in the commercial CFD code, Fluent. The numerical results agree well with the experimental data, with the largest discrepancy of 10% for the Nusselt numbers and 15% for the friction factors. The heat transfer in the DDIR tube is enhanced 100 ~ 120% compared with a plain tube and the pressure drop is increased 170 ~ 250%. The heat transfer rate for the same pumping power is enhanced 30 ~ 50%. Visualization of the flow field shows that in addition to the front and rear vortices around the ribs, main vortices and induced vortices are also generated by the ribs in the DDIR tube. The rear vortex and the main vortex contribute much to the heat transfer enhancement in the DDIR tubes. Optimum DDIR tube parameters are proposed for heat transfer enhancement at the same pumping power.

1. Introduction

Heat transfer processes are widely used in petroleum, chemical, and power generation industries. Improved heat transfer performance reduces the volume of heat exchangers and saves energy. Since the heat transfer in the tubes determines the overall heat exchanger performance, the development of efficient enhanced heat transfer tubes will significantly improve the heat exchanger efficiency. Current enhanced heat transfer tube designs use twisted tape inserts, wire coil inserts, internally finned tubes, transverse, and helical ribs, transversely and helically corrugated tubes, etc. [1]. These enhanced tubes usually result in substantially increased pressure drops for the heat transfer enhancement, so the development of new enhanced tubes with relatively lower pressure drops is important.

Guo et al. [2] first proposed the field synergy (coordination) concept that the heat transfer can be enhanced by improving the coordination between the velocity and temperature fields. This means the higher values of the integration of the dot product between the velocity vector and the temperature gradient in the area will give higher heat transfer rates. Heat transfer enhancement can be attained by increasing the magnitudes of the velocity vector and the temperature gradient or by decreasing the included angle between the velocity vector and temperature gradient. The field synergy concept gives a better understanding of many heat transfer phenomena [3–5]. More importantly, new enhanced heat transfer techniques can be developed using the field synergy principle [6]. Meng [7] analyzed the flow and temperature fields in circular tubes from the point of view of field synergy and showed that multiple longitudinal vortices provide the optimum flow pattern for heat transfer enhancement. Multiple longitudinal vortices can give the maximum heat transfer enhancement with the same viscous dissipation. The Discrete Double Incline Ribs (DDIR) tube was then developed to generate multiple longitudinal vortices [8]. Previous investigations showed that the DDIR tube has good heat transfer performance for laminar and low turbulent flow regimes. However, most working conditions for heat transfer tubes used in industry are fully turbulent condition. This paper presents the average Nusselt numbers and friction factors measured for fully turbulent flow in a DDIR tube. The flow structures and local heat transfer characteristics were numerically investigated. A parametric study of the DDIR tube performance was also conducted to improve the heat transfer.

2. Experiments

2.1. Test tube

The DDIR tube is characterized by discrete double inclined ribs on the inner tube surface as shown in Fig. 1. *Discrete* means that the ribs are not continuous as in helically finned tubes, transversely finned tubes, and spirally grooved tubes. *Double inclined* means that the ribs are not parallel or perpendicular to the flow direction but are at an inclined angle with alternating ribs inclined in opposite directions. The geometrical parameters for DDIR tubes

* Corresponding author. Tel./fax: +86 10 62773776.
E-mail address: mja@tsinghua.edu.cn (J.-a. Meng).

0017-9310/$ - see front matter © 2008 Elsevier Ltd. All rights reserved.
doi:10.1016/j.ijheatmasstransfer.2008.07.027

Nomenclature

A_i	inside tube surface area (m^2)
A_o	outside tube surface area (m^2)
A_w	nominal inside tube area, $\pi d_i L$ (m^2)
C_1	coefficient for tube side heat transfer correlation, dimensionless
C_2	constant for annular side heat transfer correlation (m^2 KW^{-1})
c_p	specific heat (J kg^{-1} K^{-1})
d_i	inside tube diameter (m)
d_o	outside tube diameter (m)
D_h	hydraulic diameter (m)
e	rib height (m)
f	friction factor, dimensionless
h	heat transfer coefficient (W m^{-2} K^{-1})
K	overall heat transfer coefficient based on outside tube area (W m^{-2} K^{-1})
L	tube length or rib length (m)
m	prandtl number exponent, dimensionless
m_i	tube side mass flow rate (kg s^{-1})
n	number of fins or Reynolds number exponent, dimensionless
Nu	nusselt number, dimensionless
p	rib pitch (m)
Pr	prandtl number, dimensionless
q	local heat flux (W m^{-2})
Q	total heat transfer rate (W)
Re	reynolds number, dimensionless
R_w	tube wall thermal resistance (K W^{-1})
T	temperature (°C)
U	volume averaged tube side flow velocity (m s^{-1})
V_o	annular side volume flow rate (m^3 s^{-1})
w	rib width (m)
X	wilson plot function (K m^2 W^{-1})
Y	variable of Wilson plot function or total thermal resistance (K m^2 W^{-1})

Greek symbols

α	rib inclined angle (°)
Δp	pressure drop (Pa)
ΔT_m	logarithmic mean temperature difference (K)
λ	thermal conductivity (W m^{-1} K^{-1})
μ	dynamic viscosity (kg m^{-1} s^{-1})

Subscripts

f	working fluid
i	inside
o	outside
w	wall

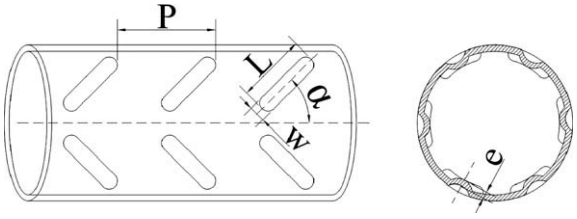

Fig. 1. Structure of the DDIR tube.

are the rib height, e, rib length, L, rib width, w, rib pitch, p, and inclination angle, α. The DDIR tube can be manufactured by pressing the discrete double inclined ribs on a plain seamless tube or by stamping the DDIR ribs on a plate and then rolling the plate into a tube and welding. The DDIR tube used in this study, which is shown in Fig. 2, was manufactured from a copper plate by stamping and rolling. The DDIR tube parameters are listed in Table 1. The tube was 2 m long.

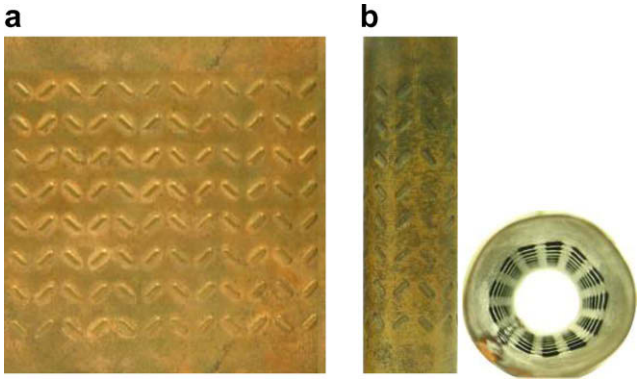

Fig. 2. Pictures of a manufactured DDIR tube. (a) DDIR plate (b) DDIR tube.

Table 1
Geometric parameters of the DDIR tube

e (mm)	α (°)	p (mm)	L (mm)	w (mm)	d_i (mm)	d_o (mm)	n
0.5	45	8.0	5.1	2.0	25.0	25.8	12

2.2. Experimental set-up

The experimental system shown in Fig. 3 included a hot water tank, a cold water tank, and the test section. The tube and annular side flow rates were measured using two flowmeters. The tube side pressure drop was measured with a differential pressure transducer. Four thermocouples were used to measure the tube and annular side inlet and outlet temperatures. The data were collected

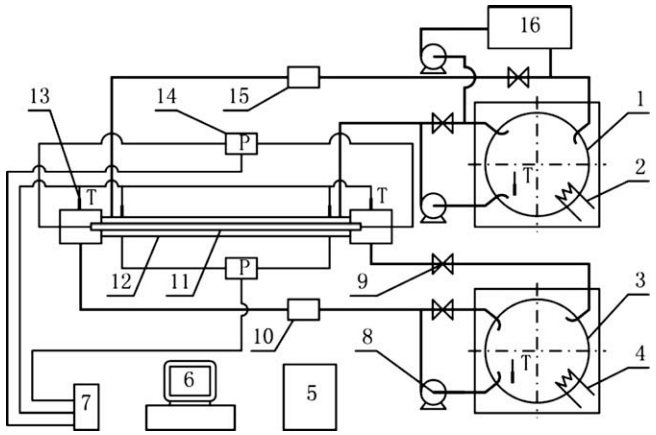

Fig. 3. Experimental system 1. cold water tank 2. auxiliary heater 3. hot water/oil tank 4. heater 5. power supply 6. computer 7. data acquisition system 8. pump 9. valve 10. Coriolis mass flow meter 11. test tube 12. test section 13. thermocouple 14. differential pressure transducer 15. turbine flow meter 16. refrigerator.

by a computer based data acquisition system. The experimental system was the same as the one used by Meng et al. [9]. The working fluid was deionized water. The tube side inlet temperature was 30 °C and the annular side inlet temperature was 15 °C.

2.3. Data reduction

The inlet and outlet temperatures and the flow rates in the tube and the annulus were used to calculate the tube side heat transfer performance. The tube side heat transfer coefficient was calculated by subtracting the annular side convective thermal resistance and the tube wall conduction thermal resistance from the total thermal resistance:

$$\frac{1}{h_i A_i} = \frac{1}{K A_o} - \frac{1}{h_o A_o} - R_w \tag{1}$$

where K is the overall heat transfer coefficient based on the outside tube area A_o, R_w is the tube wall thermal resistance, and h_o is the annular side heat transfer coefficient.

K was deduced from the total heat transfer rate and the logarithmic mean temperature difference. R_w was calculated from the geometric parameters and the thermal conductivity of copper. The annular side heat transfer coefficient, h_o, was attained using the Wilson plot technique by changing the annular side flow rate with the tube side flow rate fixed at its maximum. The annular side heat transfer coefficient can be represented by:

$$h_o = C_1 \frac{\lambda_o}{D_{h,o}} Re_o^m Pr_o^n \tag{2}$$

where the Reynolds number dependence, m, is 0.8 according to Dirker and Meyer [10] and Vilemas et al. [11]. The Prandtl number dependence, n, is 0.4 according to the popular Dittus–Boelter equation for heating. Then, the Wilson plot technique for the annular side heat transfer coefficient can be written as:

$$\frac{1}{K_o} = \frac{1}{C_1} \frac{1}{\frac{\lambda_o}{D_{h,o}} Re_o^{0.8} Pr_o^{0.4}} + C_2 \tag{3}$$

where C_1 is the coefficient in Eq. (2) and C_2 is the sum of the tube wall thermal resistance and tube side convective thermal resistance.

Then Eq. (3) can be written as:

$$Y = \frac{1}{C_1} X + C_2 \tag{4}$$

where $X = 1/[(\lambda_o/D_{h,o}) Re_o^{0.8} Pr_o^{0.4}]$, $Y = 1/K_o$.

Then C_1 can be calculated from the slope of the Wilson plot line. After determination of the coefficient in the annular side heat transfer correlation, the tube side heat transfer coefficient for various Reynolds numbers can be calculated from Eq. (1) by changing the tube side flow rate with the annulus side flow rate fixed at its maximum. The Nusselt number is then:

$$Nu = \frac{h_i d_i}{\lambda} \tag{5}$$

The friction factor is defined as:

$$f = \frac{\Delta p}{1/2 \rho U^2} \frac{d_i}{L} \tag{6}$$

The uncertainty of the measured Nusselt number was 1.8 ~ 4.4% for Reynolds numbers of 15,000–60,000, with larger uncertainties for higher Reynolds numbers due to the relatively smaller temperature differences. The uncertainty of the measured friction factor was 0.8 ~ 7.3% for Reynolds numbers of 15,000–60,000. For the low Reynolds number flow region, the uncertainty was larger due to the relatively lower flow rates.

3. Numerical simulations

3.1. Numerical model and grid distribution

As shown in Fig. 4, only one twelfth of the periodic segment was meshed for the simulations due to the symmetry of the flow. Fig. 5 shows the grid distribution, with the computational domain divided into bottom and central regions to generate a high quality grid using hexahedral elements. The grid in the bottom part containing the rib was generated along the y direction while that in the central part was generated along the x direction. An interface was used to connect the two parts where the grids are not consistent. The data were transferred by interpolation between the two regions. The elements near the walls and the ribs were smaller to insure that $y+$ was below 1. The grid was generated using Gambit 2.0. The geometric parameters in the numerical model were the same as for the tested tube listed in Table 1.

Three sets of grids with different sizes were used for the simulation to insure that the results were grid independent. The average Nusselt numbers and friction factors for the three sets of grids at a Reynolds number of 10,000 are listed in Table 2. Richardson extrapolation was used to estimate the numerical errors [12,13]. The relative difference between the estimated Nusselt number using Richardson extrapolation and the Nusselt number from the simulation using the grid with a size of 663,353 elements is 0.27%, with a relative difference for the friction factor of 0.12%. Therefore, the grid is fine enough for the simulations at Re = 10,000. The grid arrangement with 660,000 elements was used for the simulations with Reynolds numbers between 15,000 and 30,000. Simulations with higher Reynolds numbers between 40,000 and 60,000 use a grid with 1,300,000 elements.

3.2. Governing equations and turbulence modeling

The governing equations are the three-dimensional incompressible steady-state Reynolds-averaged Navier–Stokes equations and the energy equation:

Continuity:

$$\frac{\partial}{\partial x_j}(\rho u_j) = 0 \tag{7}$$

Momentum:

$$\frac{\partial}{\partial x_j}(\rho u_i u_j) = -\frac{\partial p}{\partial x_i} + \frac{\partial}{\partial x_j}\left[\mu\left(\frac{\partial u_i}{\partial x_j} + \frac{\partial u_j}{\partial x_i}\right) - (\rho \overline{u_i' u_j'})\right] \tag{8}$$

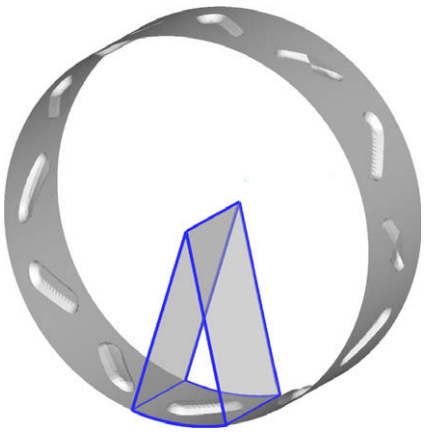

Fig. 4. One segment of the DDIR tube and the computational domain.

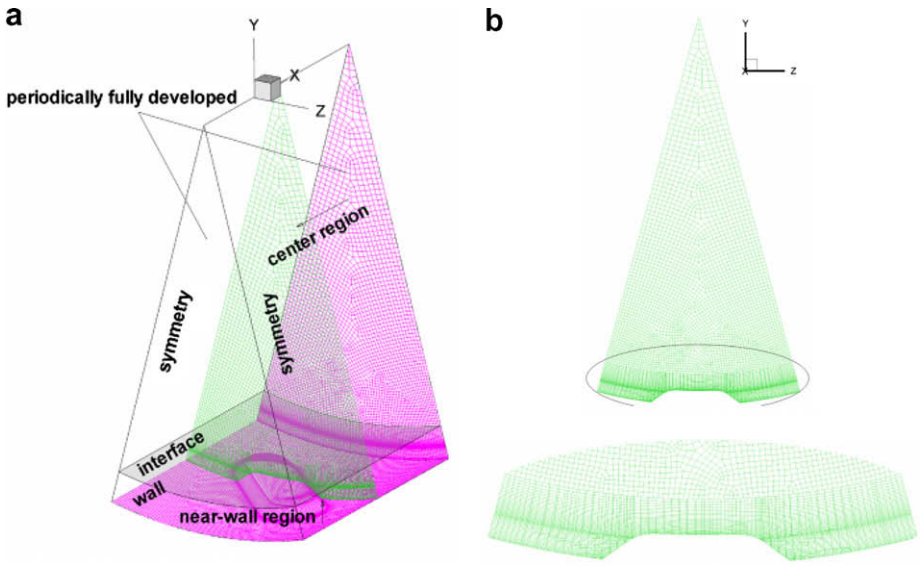

Fig. 5. Numerical model of the DDIR tube. (a) grid and boundary conditions (b) grid arrangement.

Table 2
Grid independence test and error estimate for Re = 10,000

Grid size	Nu	f
41,386	168.56	0.06180
153,756	165.55	0.06107
663,353	164.36	0.06085
Richardson extrapolation	163.93	0.06078
Relative difference (%)	0.27	0.12

Energy:

$$\frac{\partial}{\partial x_j}(\rho u_j T) = \frac{\partial}{\partial x_j}\left[\left(\frac{\mu}{Pr}+\frac{\mu_t}{\sigma_t}\right)\frac{\partial T}{\partial x_j}\right] \tag{9}$$

The standard k-ε model was used for the closure of the Reynolds stress term in Eq. (8). In the standard k-ε model, the Boussinesq hypothesis is used for modeling the Reynolds stress:

$$-\rho\overline{u_i' u_j'} = \mu_t\left(\frac{\partial u_i}{\partial x_j}+\frac{\partial u_j}{\partial x_i}\right)-\frac{2}{3}k\delta_{ij} \tag{10}$$

where the eddy viscosity is $\mu_t = \rho C_\mu \frac{k^2}{\varepsilon}$.

The transport equations for k and ε are:

$$\frac{\partial}{\partial x_i}(\rho k u_i) = \frac{\partial}{\partial x_j}\left[\left(\mu+\frac{\mu_t}{\sigma_k}\right)\frac{\partial k}{\partial x_j}\right]+G_k-\rho\varepsilon \tag{11}$$

$$\frac{\partial}{\partial x_i}(\rho\varepsilon u_i) = \frac{\partial}{\partial x_j}\left[\left(\mu+\frac{\mu_t}{\sigma_\varepsilon}\right)\frac{\partial \varepsilon}{\partial x_j}\right]+C_{1\varepsilon}G_k\frac{\varepsilon}{k}-C_{2\varepsilon}\rho\frac{\varepsilon^2}{k} \tag{12}$$

where $G_k = -\rho\bar{u}_i' u_j' \frac{\partial u_j}{\partial x_i}$ represents the production of turbulent kinetic energy, $C_{1\varepsilon}$ = 1.44, $C_{2\varepsilon}$ = 1.92, C_μ = 0.09, σ_k = 1.0, σ_ε = 1.3 and the turbulent Prandtl number, σ_t, in Eq. (9) is 0.85.

The governing equations were solved using the commercial CFD code, Fluent 6.0. This program uses the finite volume method with a cell centered grid. The SIMPLEC algorithm was used for the velocity–pressure coupling. The QUICK scheme was used for the discretization of the convective terms. The grid was fine enough near the tube wall that the two-layer zone model was used for the near wall turbulence modeling.

3.3. Boundary conditions

As shown in Fig. 5 (a), the periodically fully developed condition was used for the inlet and outlet cross sections with symmetry used for the two sides. The non-slip condition with constant wall temperature was used for the tube wall. The periodically fully developed condition means that the pressure and the velocity components repeat themselves in the stream wise direction as:

$$\vec{u}(\vec{r}) = \vec{u}(\vec{r}+\vec{L}) = \vec{u}(\vec{r}+2\vec{L}) = \cdots \tag{13}$$

$$\Delta p = p(\vec{r}) - p(\vec{r}+\vec{L}) = p(\vec{r}+\vec{L}) - p(\vec{r}+2\vec{L}) = \cdots \tag{14}$$

The temperature was normalized as:

$$\theta = \frac{T(x,\vec{r})-T_{\text{wall}}}{T_{x,b}-T_{\text{wall}}} \tag{15}$$

where $T_{x,b} = \frac{\int_{A_x} T|\rho\vec{u}\cdot d\vec{A}|}{\int_{A_x}|\rho\vec{u}\cdot d\vec{A}|}$.

Then the periodic condition for the normalized temperature with constant wall temperature condition can be expressed as:

$$\theta(\vec{r}) = \theta(\vec{r}+\vec{L}) = \theta(\vec{r}+2\vec{L}) = \cdots \tag{16}$$

The working fluid in the numerical simulation was constant property water.

4. Results and discussion

4.1. Average Nusselt numbers and friction factors

The tube length average Nusselt numbers and friction factors in the DDIR tube are shown in Fig. 6. The rectangular symbols represent the experimental results while the circular symbols represent the numerical results. The average Nusselt numbers and friction factors in plain tubes in Fig. 6 are calculated using Gnielinski [16] and Filenenko [17] equations. The heat transfer coefficients from the numerical simulation were defined as:

$$h = \frac{Q}{A_w \Delta T_m} \tag{17}$$

$$q = \lambda\left.\frac{\partial T}{\partial r}\right|_w \tag{18}$$

where $Q = \int_A q dA$ is the total heat transfer rate, A_w is the nominal inside tube area, ΔT_m is the logarithmic mean temperature difference, and q is the local heat flux.

Then the Nusselt number was calculated as in Eq. (5). The friction factors were calculated as in Eq. (6). Fig. 6(a) shows the Nusselt numbers for the DDIR tube, with the relative differences between the experimental and numerical results being

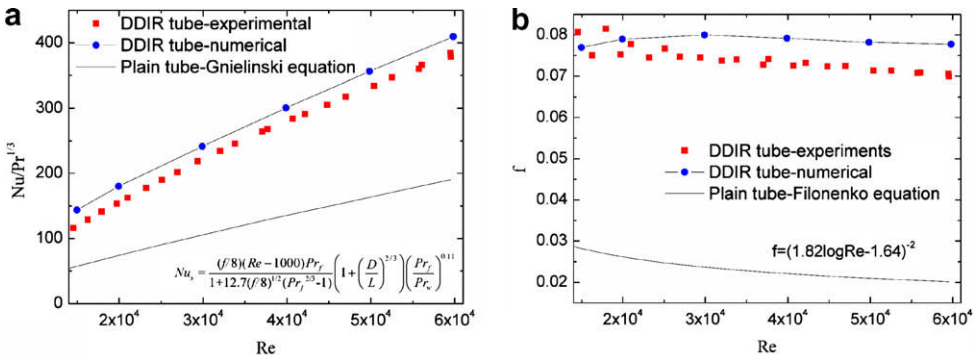

Fig. 6. Flow and heat transfer performance of the DDIR tube for Re = 15,000–60,000. (a) Nusselt number (b) friction factor.

below 10%. The heat transfer in the DDIR tube is enhanced by 100 ~ 120% compared with a plain tube at Reynolds numbers between 15,000 and 60,000. Fig. 6(b) shows the experimental and predicted friction factors with relative differences below 15%. The friction factors in the DDIR tube are 170 ~ 250% higher than in a plain tube at Reynolds numbers between 15,000 and 60,000. The roughness of the welding line on the tested tube is a key reason for the differences between the numerical and experimental results.

There are many types of enhanced heat transfer tubes, but they generate large pressure drops while enhancing heat transfer, which means large pumping powers. From the point of view of energy saving, the performance evaluation criteria, $PEC = (Nu/Nu_0)/(f/f_0)^{1/3}$, is used to evaluate the enhanced heat transfer performance at the same pumping power. Fig. 7 shows the PECs of the DDIR tube and two other commonly used enhanced tubes at Reynolds numbers between 15,000 and 60,000. The Nusselt numbers and friction factors for the other two tubes were calculated from empirical correlations. The Nusselt number and friction factor correlations for the spirally corrugated tube are given by Vicente et al. ($e/d_i = 0.07$, $p/d_i = 2.68$) [14]. The Nusselt number and friction factor correlations for the wire coil inserts are given by Garcia et al. ($e/d_i = 0.06$, $p/d_i = 1$) [15]. Fig. 7 shows that the heat transfer enhancement at the same pumping power for the DDIR tube is 30 ~ 50% higher than for a plain tube for Reynolds numbers between 15,000 and 60,000. The PECs for the DDIR tube are higher than for the spirally corrugated tube and the tube with wire coil inserts.

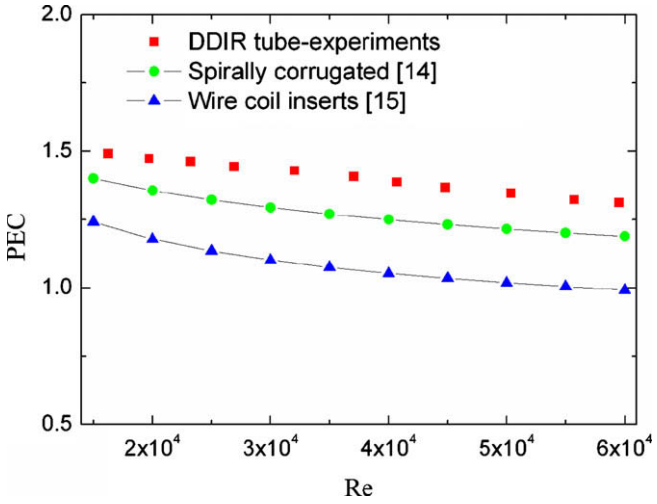

Fig. 7. PECs for various enhanced tubes.

4.2. Flow structure and local heat transfer characteristics

The flow structure in the DDIR tube is visualized in Figs. 8 and 9. Fig. 8 shows the streamlines around a rib in the DDIR tube, which show two vortices around the rib. One is a vortex in front of the rib, called the front vortex, while the other is a vortex behind the rib, called the rear vortex. The helical streamlines show that the rear vortex is much stronger than the front vortex. Fig. 9 shows the predicted tangential velocity vectors in the outlet cross section at a Reynolds number of 30,000. The velocity vectors in Fig. 9 shows a large vortex not shown in Fig. 8, called the main vortex. The vortex core is near the tube wall and the tangential velocity magnitude is higher in the near wall region than in the central region which will cause larger velocity gradients near the tube wall. The maximum tangential velocity in the cross section is as much as 5% of the average main stream velocity. The right corner of Fig. 9 has a small induced longitudinal vortex beside the main vortex. Thus the rib created four vortices, the front vortex, the rear vortex, the main vortex, and the induced vortex. These vortices greatly enhance the heat transfer in the DDIR tube.

Fig. 10 shows the isotherms at the outlet cross section of the DDIR tube and a plain tube at a Reynolds number of 30,000. The continuous lines are the isotherms in the DDIR tube and the dotted lines are the undisturbed isotherms in a plain tube. Comparison of the two sets of temperature contours shows that the temperature field in the DDIR tube is changed dramatically by the longitudinal vortex. The temperature gradients are larger where the tangential velocities flow towards the tube wall, while in the left corner where the tangential velocity flows away from the tube wall, the temperature gradients are small. Thus the main vortex in this cross section greatly enhances the heat transfer.

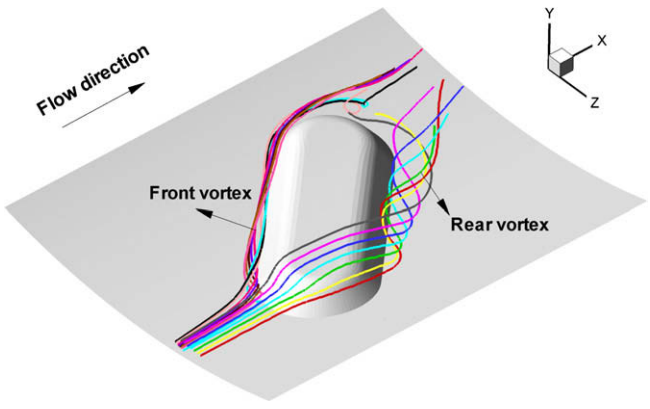

Fig. 8. Streamlines around a rib.

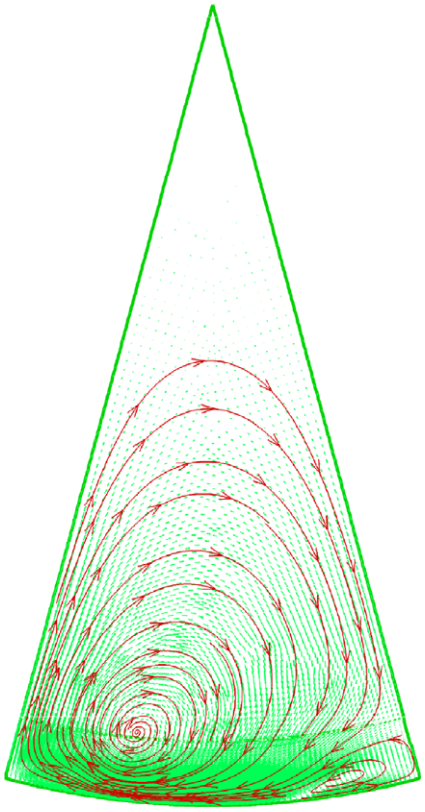

Fig. 9. Tangential velocity vectors and streamlines in the outlet cross section at *Re* = 30,000.

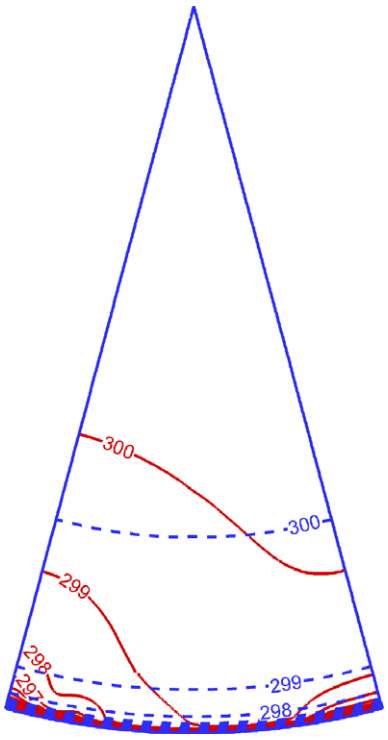

Fig. 10. Isotherms in the outlet cross section at *Re* = 30,000.

Figs. 11 and 12 show the local Nusselt numbers at the outlet cross section and on the DDIR tube surface. The local Nusselt numbers are defined as:

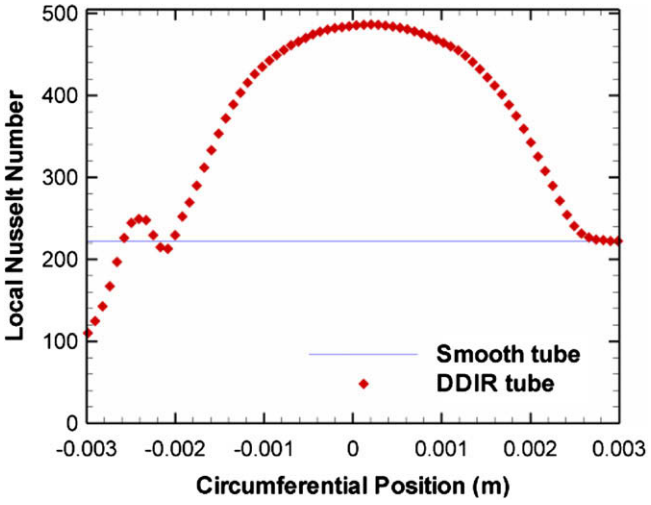

Fig. 11. Local Nusselt numbers at *Re* = 30,000.

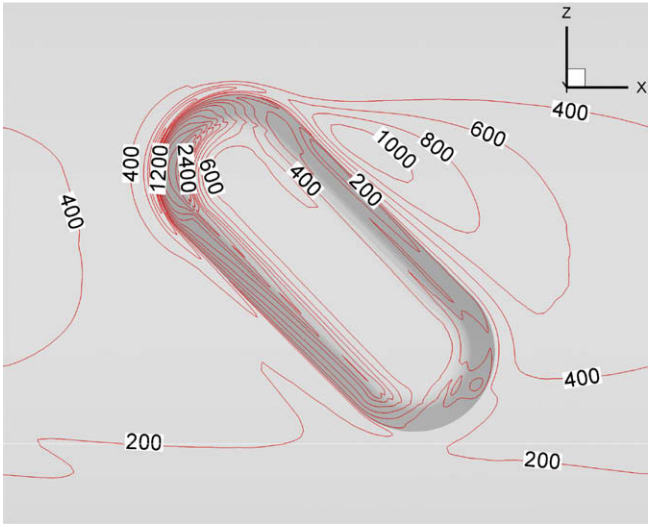

Fig. 12. Local Nusselt numbers on the tube surface at *Re* = 30,000.

$$h_{\text{local}} = \frac{q}{T_w - T_f} \tag{19}$$

$$Nu = \frac{h_{\text{local}} d_i}{\lambda} \tag{20}$$

where q is defined as in Eq. (18).

Fig. 11 shows the local Nusselt numbers along the circumference of the outlet cross section at a Reynolds number of 30,000. The maximum heat transfer occurs where the flow is towards the tube wall. The synergy between the velocity vector and the temperature gradient is much improved in this area. The local heat transfer is as high as 2.3 times that in a plain tube. The heat transfer in the left corner is reduced as the fluid flows away from the tube wall and the synergy between the velocity vector and temperature gradient are poor. The average of the local Nusselt numbers shown in Fig. 11 is 1.6 times that in a plain tube for the same condition. Fig. 12 shows that the local Nusselt numbers on the DDIR tube surface at a Reynolds number of 30,000 are much higher on the front surface of the ribs. This is due to the fluid impacting the front surface of the ribs, so that the included angle between the velocity vector and temperature gradient is very small. The local Nusselt numbers are also higher on the tube surfaces after

the ribs where the rear vortex and the main vortex increase the synergy between the velocity vectors and the temperature gradients in this region. The enhanced heat transfer area on the front surface of the ribs is much smaller than on the tube surfaces after the ribs, so the contribution to the total heat transfer enhancement of the area on the front surface of the ribs is less than the tube surface area after the ribs. Therefore, the heat transfer enhancement in the DDIR tubes is mainly caused by the rear vortex and the main vortex. In the enhanced heat transfer area after the ribs, the enhancement is much higher right after the ribs than further downstream from the ribs, which implies that the rib pitch influences the heat transfer in the DDIR tube.

4.3. Parametric study of the DDIR tube performance

Industrial applications need to know the optimum DDIR tube geometric parameters and also the heat transfer and flow friction performances for other tube parameters. The influences of the rib height, e, the number of ribs around the circumference, n, and the rib pitch, p, on the DDIR tube performance was studied numerically. The Nusselt number ratios, friction factor ratios and PECs for a Reynolds number of 20,000 are presented for various rib heights, numbers of ribs around the circumference, and rib pitches in Figs. 13–15. Nu_e and f_e represent the Nusselt number and friction factor in the DDIR tube. Nu_0 is the Nusselt number in a plain tube calculated using the Gnielinski equation [16], while f_0 is the friction factor in a plain tube calculated using the Filonenko equation [17]. The rib height is the most important parameter. Fig. 13(a) shows the Nusselt number ratios and the friction factor ratios in the DDIR tube with rib heights from 0.25 to 1.25 mm, corresponding to $1 \sim 5\%$ of the tube diameter, for 12 ribs (or 6 pairs) around the circumference and a rib pitch of 8 mm. At rib heights less than 0.5 mm, the friction factor ratio is comparable to the Nusselt number ratio. The heat transfer rate and the pressure drop both increase about 30% at a rib height of 0.23 mm. However, the heat transfer is enhanced 95% while the pressure drop is increased 145% for a rib height of 0.46 mm. For rib height greater than 0.75 mm, the friction factor ratios increase much more rapidly than the Nusselt number ratios with a Nusselt number ratio of 2.7 and a friction factor ratio of 4.9 for a rib height of 0.75 mm. While the Nusselt number ratio at a rib height of 1.25 mm is 3.3 while the friction factor ratio is 10.9. Fig. 13(b) shows that the highest PEC is 1.56 for a rib height of 0.75 mm. The PECs are lower at rib heights higher than 0.75 mm due to the large pressure drop ratios and are lower at rib heights less than 0.75 mm due to the relatively small heat transfer enhancement. Therefore, the optimum rib height for energy conservation is around 0.75 mm, which corresponds to 3% of the tube diameter. Lower or higher rib heights

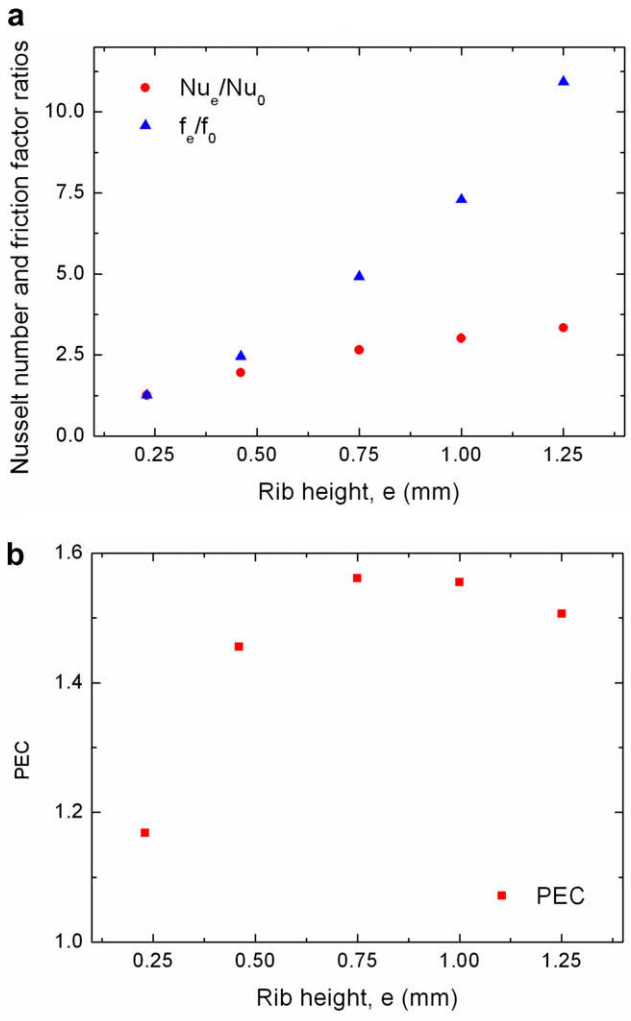

Fig. 13. DDIR tube performance with 12 rib around the circumference and a rib pitch of 8 mm at $Re = 20{,}000$. (a) Nusselt number and friction factor ratios for various rib heights (b) PECs for various rib heights.

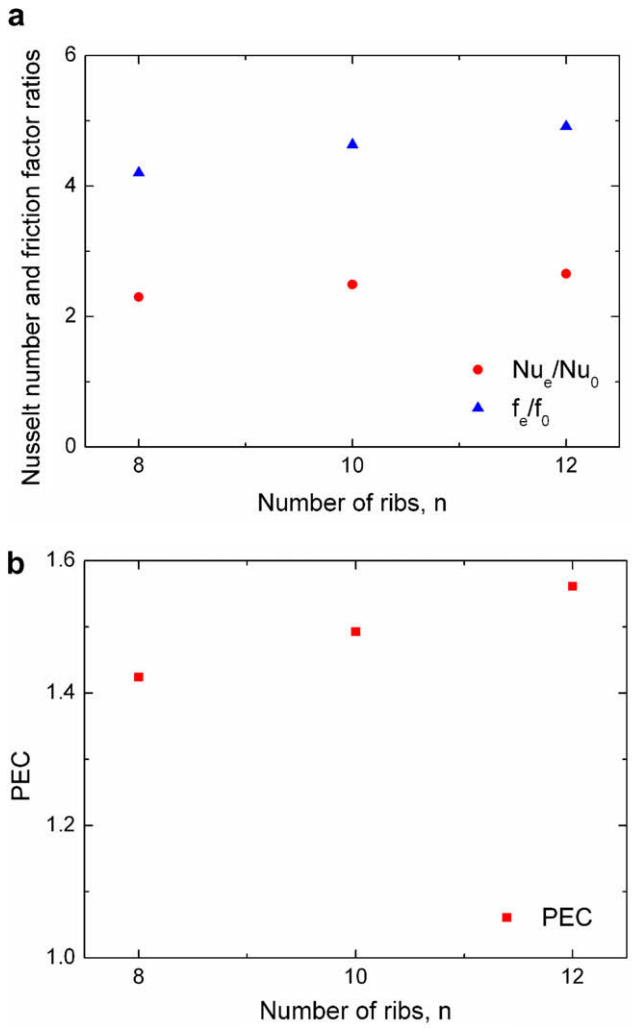

Fig. 14. DDIR tube performance for a rib height of 0.75 mm, a rib pitch of 8 mm at $Re = 20{,}000$. (a) Nusselt number and friction factor ratios for various numbers of ribs (b) PECs for various numbers of ribs.

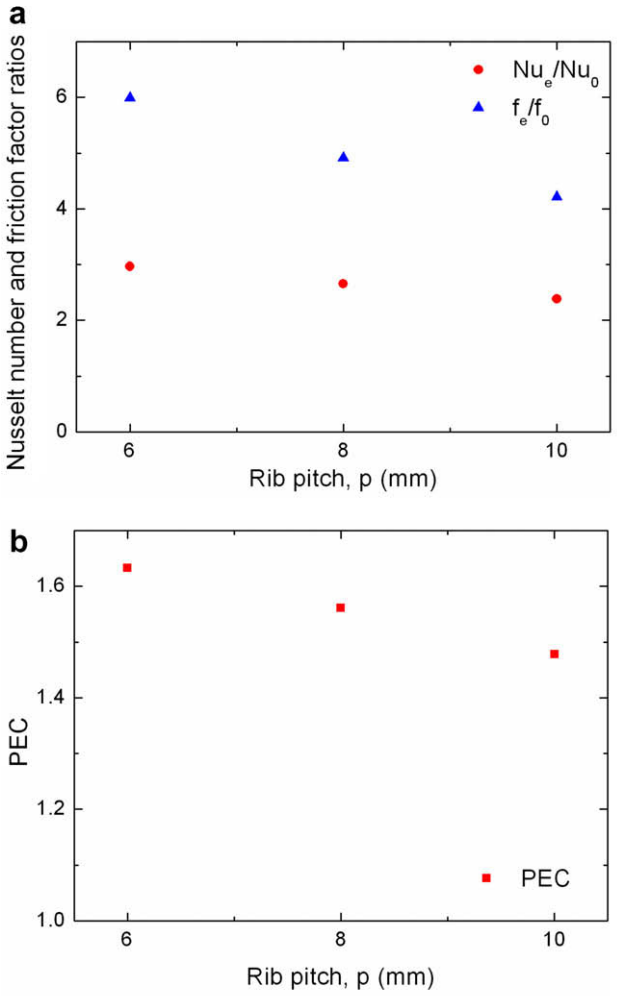

Fig. 15. DDIR tube performance for a rib height of.75 mm, 12 ribs around the circumference at $Re = 20{,}000$. (a) Nusselt number and friction factor ratios for various rib pitches (b) PECs for various rib pitches.

can be used when aiming at reducing the pumping power or increasing the heat transfer enhancement.

Fig. 14 shows the DDIR tube heat transfer and friction factor ratios for 8, 10, and 12 ribs around the circumference for a rib height of 0.75 mm and a rib pitch of 8 mm. From Fig. 14(a), the Nusselt number ratios and the friction factor ratios both increase slightly with increasing number of ribs since the total enhanced area is increased by increasing the number of ribs. The PECs shown in Fig. 14(b) increase from 1.42 to 1.56 as the numbers of ribs increases from 8 to 12, so the DDIR tube performance is better with more ribs. A maximum rib number of 12 is proposed for applications due to the difficulty of manufacturing DDIR tubes with many ribs.

Fig. 15 shows the DDIR tube heat transfer and friction factor ratios for rib pitches of 6, 8, and 10 mm for a rib height of 0.75 mm and 12 ribs around the circumference. The Nusselt number ratios and the fiction factor ratios both decrease with increasing rib pitch. Fig. 15(b) shows that the PECs for the DDIR tube decrease with increasing rib pitch. This is due to the heat transfer rate at the area right behind the ribs is much higher than the average, so increase in the rib pitch means increasing the more effective heat transfer areas. The smallest ribs pitch of 6 mm is recommended for applications.

5. Conclusions

The heat transfer and pressure drop in a DDIR tube were experimentally and numerically studied for a range of geometries and flow conditions. The average Nusselt numbers and friction factors along the tube from the numerical simulations agree well with the experimental data. The predicted flow fields were used to analyze the flow structures and the local heat transfer characteristics. The influences of the rib height, the number of ribs and the rib pitches on the DDIR tube performance were numerically investigated. The main conclusions are:

1. Compared to a plain tube, the DDIR tube enhances the heat transfer by $100 \sim 120\%$ and increases the pressure drop by $170 \sim 250\%$ at Reynolds numbers between 15,000 and 60,000. The heat transfer rate for the same pumping power in the DDIR tube is $30 \sim 50\%$ higher than in a plain tube and is higher than in commonly used enhanced tubes, such as, tubes with wire coil inserts or spirally corrugated tubes.
2. The numerical results show four kinds of vortices in the DDIR tube, a front vortex, a rear vortex, a main vortex, and an induced vortex. It is these vortices that greatly increase the heat transfer in DDIR tube.
3. The parametric study shows that there is an optimum PEC at a rib height of 3% of the tube diameter, which is 0.75 mm for the tube used in this analysis. The PECs increase with number of ribs around the circumference and decrease with increasing rib pitches. Practical tubes are recommended to have 12 ribs and a rib pitch of 6 mm.

Acknowledgement

This work was financially supported by the National Basic Research Program of China (Grant Nos. G2000026301 and 2007CB206901).

References

[1] R.L. Webb, Principles of Enhanced Heat Transfer, John Wiley Sons, New York, 1994.
[2] Z.Y. Guo, D.Y. Li, B.X. Wang, A novel concept for convective heat transfer enhancement, Int. J. Heat Mass Transfer 41 (14) (1998) 2221–2225.
[3] Z.Y. Guo, Mechanism and control of convective heat transfer – Coordination of velocity and heat flow fields, Chin. Sci. Bull. 46 (7) (2001) 596–599.
[4] W.Q. Tao, Z.Y. Guo, B.X. Wang, Field synergy principle for enhancing convective heat transfer – its extension and numerical verifications, Int. J. Heat Mass Transfer 45 (18) (2002) 3849–3856.
[5] Y.L. He, W.Q. Tao, F.Q. Song, W. Zhang, Three-dimensional numerical study of heat transfer characteristics of plain plate fin-and-tube heat exchangers from view point of field synergy principle, Int. J. Heat Fluid Flow 26 (3) (2005) 459–473.
[6] Z.Y. Guo, W.Q. Tao, R.K. Shah, The field synergy (coordination) principle and its applications in enhancing single phase convective heat transfer, Int. J. Heat Mass Transfer 48 (9) (2005) 797–1807.
[7] J.A. Meng, Enhanced Heat Transfer Technology of Longitudinal Vortices Based on Field-coordination Principle and Its Application, PhD Thesis, Tsinghua University, Beijing, 2003.
[8] J.A. Meng, X.G. Liang, Z.X. Li, Field synergy optimization and enhanced heat transfer by multi-longitudinal vortices flow in tube, Int. J. Heat Mass Transfer 48 (16) (2005) 3331–3337.
[9] J.A. Meng, X.G. Liang, Z.J. Chen, Z.X. Li, Experimental study on convective heat transfer in alternating elliptical axis tubes, Exp. Therm. Fluid Sci. 29 (4) (2005) 457–465.
[10] J. Dirker, J.P. Meyer, Convective heat transfer coefficients in concentric annuli, Heat Transfer Eng. 26 (2) (2005) 38–44.
[11] J. Vilemas, B. Cesna, V. Survila, Heat Transfer in Gas-cooled Annular Channels, Hemisphere Publishing, Washington, 1987.
[12] P.J. Roach, Perspective – a method for uniform reporting of grid refinement studies, ASME J. Fluid Eng. 116 (3) (1994) 405–413.
[13] W.Q. Tao, Recent Advances in Computational Heat Transfer, Science Press, Beijing, 2001 (in Chinese).

[14] P.G. Vicente, A. Garcia, A. Viedma, Experimental investigation on heat transfer and frictional characteristics of spirally corrugated tubes in turbulent flow at different Prandtl numbers, Int. J. Heat Mass Transfer 47 (4) (2004) 671–681.
[15] A. Garcia, P.G. Vicente, A. Viedma, Experimental study of heat transfer enhancement with wire coil inserts in laminar-transition-turbulent regimes at different Prandtl numbers, Int. J. Heat Mass Transfer 48 (21–22) (2005) 4640–4651.
[16] V. Gnielinski, New equations for heat and mass transfer in turbulent pipe and channel flows, Int. Chem. Eng. 16 (2) (1976) 359–368.
[17] V. Gnielinski, Single-phase Convective Heat Transfer, Hemisphere, New York, 1983.